J. Fluid Mech. (1972), *vol.* 52, *part* 3, *pp.* 401–423
Printed in Great Britain

Experimental investigations of the stability of channel flows. Part 2. Two-layered co-current flow in a rectangular channel

By TIMOTHY W. KAO AND CHEOL PARK

Department of Aerospace and Atmospheric Sciences,
The Catholic University of America

(Received 1 September 1970 and in revised form 7 September 1971)

The stability of the laminar co-current flow of two fluids, oil and water, in a rectangular channel was investigated experimentally, with and without artificial excitation. For the ratio of viscosity explored, only the disturbances in water grew in the beginning stages of transition to turbulence. The critical water Reynolds number, based upon the hydraulic diameter of the channel and the superficial velocity defined by the ratio of flow rate of water to total cross-sectional area of the channel, was found to be 2300. The behaviour of damped and growing shear waves in water was examined in detail using artificial excitation and briefly compared with that observed in Part 1. Mean flow profiles, the amplitude distribution of disturbances in water, the amplification rate, wave speed and wavenumbers were obtained. A neutral stability boundary in the wavenumber, water Reynolds number plane was also obtained experimentally.

It was found that in natural transition the interfacial mode was not excited. The first appearance of interfacial waves was actually a manifestation of the shear waves in water. The role of the interface in the transition range from laminar to turbulent flow in water was to introduce and enhance spanwise oscillation in the water phase and to hasten the process of breakdown for growing disturbances.

1. Introduction

In part 1 of this study, Kao & Park (1970) (hereafter referred to as Part 1), the stability of the laminar flow of water in a rectangular channel was reported. Natural disturbances as well as artificially excited disturbances were studied. In the present work, which forms part 2 of this research, the stability of the laminar co-current flow of oil and water is examined in detail using the same channel, whose overall aspect ratio $H:B$ (depth:width) is 1:8. In all the experiments presented here the two layers are kept at equal depths.

The mean flow profile for a two-layered co-current flow in a rectangular channel may be easily calculated, and was first given by Tang & Himmelblau (1963). In our case, calculations show that the mean flow in the spanwise mid-section of width 4 in. is two-dimensional, i.e. in that range there is no spanwise variation and the mean flow profile coincides with that of simple two-layered plane Poiseuille flow. The stability problem for the latter flow subject to infinitesimal

two-dimensional disturbances has been formulated by Yih (1967). On decomposing the disturbance into normal modes the governing equations become the Orr–Sommerfeld equations for the two layers. These are to be solved subject to no-slip conditions at the upper and lower walls, together with the continuity of velocity and shear stress, and the balance of normal stresses (including that induced by surface tension) at the interface. The whole system of equations forms an eigenvalue problem. Two different approaches may be adopted in the normal-mode method. The disturbances may be examined for temporal or spatial growth (decay) according to whether the frequency parameter or wavenumber parameter is considered to be complex. In common with all other experimental work of this nature, our study is concerned with the spatial problem and the data will be presented accordingly. That is, α is complex ($\alpha = \alpha_r + i\alpha_i$) and β is real in the factor $\exp\{i(\alpha x - \beta t)\}$, where $\alpha_r\,(= 2\pi h/\lambda$, with λ denoting the wavelength) is the dimensionless wavenumber and x is the dimensionless horizontal distance along the length of the channel, both being normalized by h, the half-depth of the channel, $\beta(= 2\pi f h/U_m$, with f denoting the frequency) is the dimensionless frequency parameter and t is the dimensionless time, both being normalized by h/U_m, where U_m is the average velocity of water and is defined in §2. $-\alpha_i$ is the amplification coefficient:

$$\alpha_i = -2{\cdot}3\frac{d}{dx}\left(\log_{10}\frac{u'}{u'_0}\right),$$

where u' is the root–mean–square value of u, the instantaneous x component of fluctuation velocity, and u'_0 is a reference value of u' at a fixed horizontal position.

For this study it may be advantageous to classify the disturbances into two types: (i) shear waves in the fluids, (ii) interfacial waves at the interface. These may be distinguished by their amplitude distribution with depth; the interfacial wave has an amplitude which is a maximum at the interface and which falls off monotonically away from the interface. It is important to realize that the shear waves will disturb the interface sufficiently to cause the interface to manifest waviness, so that whether a truly interfacial wave is excited or not cannot be ascertained by merely observing the interface, nor can one infer the mechanics of energy transfer to interfacial disturbances through such observations. As noted in Part 1, the appearance of interfacial waves was first observed by Charles & Lilleleht (1965).

The theoretical problem outlined earlier is rather complex and will not be attempted here. Instead the stability problem will be investigated experimentally and the neutral stability curve in the β, R and α_r, R planes, where R is a Reynolds number, will be determined experimentally. It should be pointed out that the interfacial mode and the shear modes in water may become unstable separately. In that case two neutral stability curves would be obtained. However, as will be seen later, this did not turn out to be the case with the present system. It appears that, with the ratio of viscosity in our experiment, only the disturbances in water grew in the beginning stages of transition to turbulence. This possibility of disturbances growing in only one fluid while damped in the other was first noted by Lock (1954) in a theoretical study of boundary layer between two different

fluids. It should also be noted that Yih (1967) has solved the temporal stability problem of this two-layered flow in the long-wave limit and has included numerical values for the special case where the two fluids have the same density. He found a long-wave instability at the interface at low Reynolds numbers. In the present investigation the two liquids have unequal densities and such an instability was not detected for the range of Reynolds numbers tested.

The major effort of this study is to investigate experimentally the detailed behaviour of the disturbances excited by artificial excitation in the range of transition from laminar to tubulent flow. Measurements at the interface were also made. A hot-film technique was applied to measure the mean flow velocities and the disturbances; interfacial motion was measured by means of a wave gauge. All measurements of the disturbances by the hot film were performed in water only. In the range of flow tested the oil remained fully laminar. Thus only the water layer underwent transition to turbulence. The neutral stability boundary was obtained.

2. Experimental set-up and procedure

The experimental set-up is shown in figure 1. The main channel was the same as that in Part 1. The flow was maintained by constant-head tanks for both water and oil and was re-circulated by pumps. Each tank was provided with an overflow device to maintain a constant head. Two parallel on-line water filters capable of filtering the water down to 40 μm were installed ahead of a water flow-rate meter. An ordinary automobile engine oil filter with a little modification was connected between the constant-head tank for oil and an oil flow-rate meter. The inlet section was divided into two parts by thin copper plate so that the two liquids came in separately without mixing, and any large eddy in either part was reduced through a section with plastic drinking straws 0·059 in. in diameter and bounded on each side by a fine mesh screen. The flow was allowed to mix during discharge from the channel and the mixture was separated in the separation tank. The head in the separation tank was kept constant by the overflow of oil and by using an interface sensing probe. The probe consisted of three copper rods $\frac{1}{16}$ in. in diameter connected to an electronic device which operated the on–off solenoid valve for fresh tap water. Using this device, the interface in the separation tank was kept to within $\frac{1}{8}$ in. deviation from its mean position. The discharged water was continuously by-passed to give a constant temperature and greater purity to the water in the system. The flow rate as well as the temperature was kept steady. The temperature was monitored by thermometers at different points in the system. The working fluids were ordinary tap water and a light mineral oil (Diala-AX) supplied by Shell Oil Company (ratio of viscosity of this oil to water is 20, specific gravity 0·864 at 55 °F, see Shell Oil Co. Technical Bulletin L-26-1 for technical details).

Measurements of the mean flow profiles and disturbances in both water and oil were made by means of hot-film anemometers in the same manner as that reported in Part 1. The disturbance generator was also the same as that in Part 1. A wave gauge was used to measure the wave speed and damping (or growth)

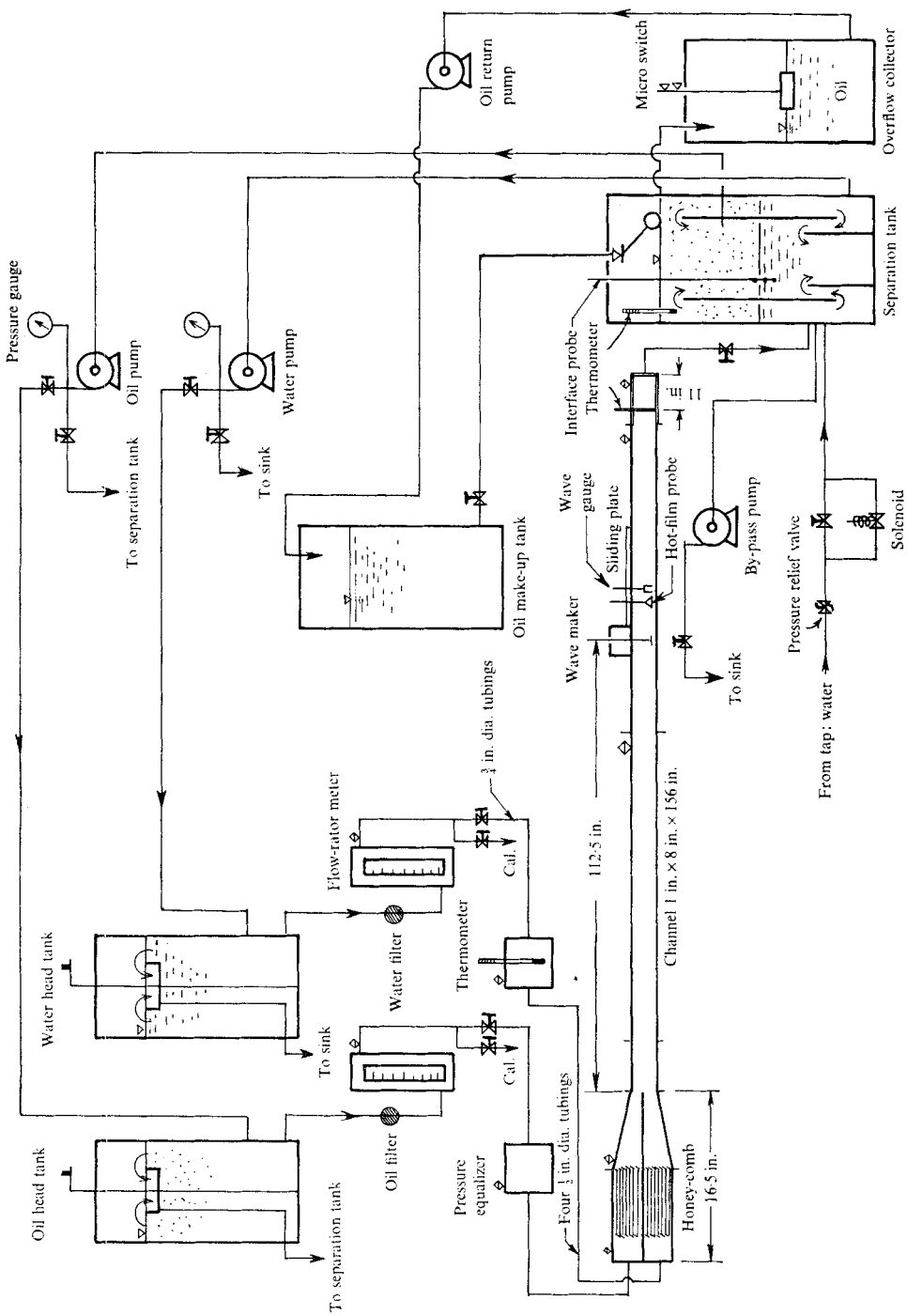

FIGURE 1. The experimental set-up.

rate of interfacial waves. The wave gauge consisted of two submerged vertical parallel copper wires (1·2 in. apart, 0·95 in. long, 0·01 in. diameter). Since water is conducting and this oil is non-conducting, the change in the resistance between the two wires of the wave gauge was proportional to the depth of oil in the channel. Thus the interfacial motion could be detected by measuring the voltage output across a fixed resistor (10 kΩ).

The procedure followed in the experiments was the same as that reported in Part 1 (see also Park & Kao (1970) for a more detailed description). In the present work, the Reynolds number for each fluid is defined as $R = U_s d/\nu$, where U_s is the superficial velocity (defined by the ratio of the flow rate Q of water or oil to the total cross-sectional area A of the channel), d is the hydraulic diameter ($d \equiv 4A/C$, where C denotes the wetted perimeter) and ν is the kinematic viscosity. In this experiment, with $A = 8\,\text{in.}^2$ and $C = 18\,\text{in.}$, the following relationships were used to determine the Reynolds numbers:

$$R_w = 5{\cdot}94 \times 10^{-3} Q_w/\nu_w,$$
$$R_o = 5{\cdot}94 \times 10^{-3} Q_o/\nu_o,$$

where the subscripts w and o denote water and oil respectively, with the discharges measured in gallons/min and viscosities in ft²/s. The kinematic viscosity was taken from the value given by the Shell Oil Co. Bulletin L-26-1 for the oil and from the value shown in the handbook by King (1954) for the pure water. As a check, the dynamic viscosity of the oil was measured by using a viscosimeter (Stormer) and the specific gravity of the oil was obtained from a hydrometer for different temperatures.

The mean flow average velocity for the water phase was obtained from the water flow-rate meter reading, using the relation $U_m = Q_w/S$, where S is the wetted cross-sectional area ($S = 4\,\text{in.}^2$). Mean flow profiles of water and oil were measured for different Reynolds numbers by using the hot-film probes at a position 3 in. behind the ribbon of the wave maker, where the flow was estimated to be fully developed for the Reynolds numbers explored. The mean flow velocity measured by the hot film at $Y = 0{\cdot}25\,\text{in.}$, where Y denotes the vertical distance through the depth of the channel measured from the bottom, was taken as the approximate maximum value of the mean velocities and was denoted by U_c. This position is also approximately the theoretical location for maximum velocity. A depth gauge with a resolution of $\frac{1}{1000}$ in. was used to check the depth ratio and enabled the interface to be located to within 2 % of the channel depth even under dynamic conditions. In all the experiments, the ratio of the depth of oil to water was maintained at unity by adjusting the discharges.

For measurements of the mean flow the probes were calibrated before and after each test and inserted from the bottom and the top for measurements in water and oil respectively. Velocities away from the interface were measured by the hot-film probes in the two layers and the velocity near the interface was checked by timing tiny air bubbles immediately below the interface. These tiny air bubbles were made by injecting a small amount of air into water using a syringe. The lack of data precisely at the interface introduced some error in the non-dimensional mean flow velocity profile especially at higher Reynolds numbers when the mean flow

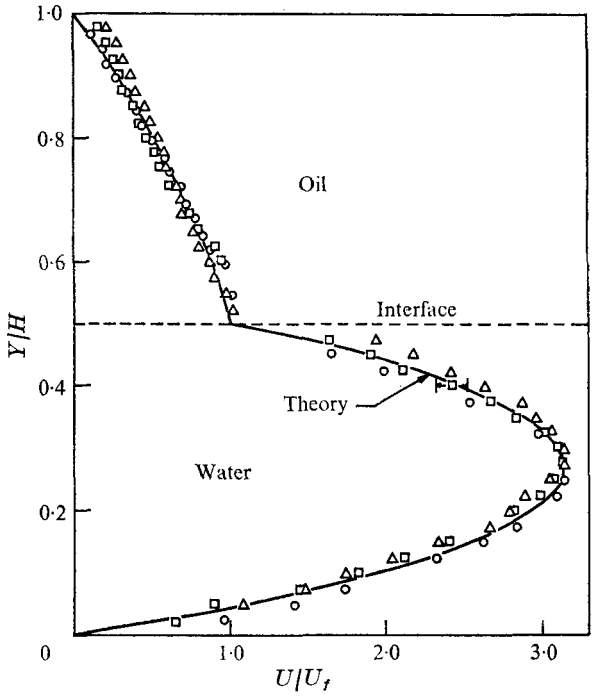

FIGURE 2. Mean flow profiles when the ratio of viscosity of oil to water is 20. Solid line represents the theoretical curve. ○, $R_w = 750$, $R_o = 16$; □, $R_w = 1280$, $R_o = 25$; △, $R_w = 1880$, $R_o = 36$. Bar denotes the uncertainties.

oil data became less accurate owing to entrainment of microscopic air bubbles in the oil phase, resulting in a slight change in the hot-film response from calibration conditions. A typical uncertainty is illustrated by a bar in figure 2.

Interfacial surface tension was measured by the Pendant Drop Method introduced by Andreas, Hauser & Tucker (1938) and used by Fordham (1948). Photographs of pendant drops of water surrounded by oil were taken using a 4 in. by 5 in. polaroid camera. The interfacial surface tension between water and oil was found to be 30·2 dynes/cm at 75 °F.

The experimental procedure for flow measurements with artificial excitations was described in Part 1. Except for the mean flow measurement, no hot-film measurement was performed in oil because most of the disturbances there were too rapidly damped to be measured. The disturbances were surveyed in water by the hot-film probe placed depthwise and longitudinally downstream of the ribbon from $X = 3{\cdot}5$ in. to $X = 11{\cdot}5$ in. along the spanwise centre-line ($Z = 0$), where X is the horizontal distance along the length of the channel measured downstream from the ribbon and Z is the horizontal distance across the width of the channel measured from the spanwise centre-line. It may be noted in figure 1 that a modification was made in the position of the wave maker relative to the sliding plate, so that the closest approach of the probe to the ribbon was 3·5 in. in this paper as compared with 13 in. in Part 1. The total length of travel for the probe however remained unchanged. Such experiments were done for increasing

Reynolds numbers. In the range of Reynolds numbers where the flow began to be unstable, the interface became distinctly wavy and natural disturbances appeared in turbulent spots or bursts even with the exciter off.

The interfacial wave speed was measured by recording signals from the wave gauge and the signal from the LVDT simultaneously, as in the second method of wave speed measurement described in §2 of Part 1. As in Part 1, portions of the data were digitized and then Fourier analysed on a digital computer (IBM 1130) for spectral components.

3. Experimental results and discussion

Mean flow velocity profiles were obtained by means of hot-film measurements at the fully laminar range for several low flow rates at $X = 3{\cdot}0$ in., where a probe insertion station, apart from the sliding-plate mechanism, is located. No detectable difference in the mean flow was found when the ribbon was in place at 0·05 in. from the bottom of the channel. The ribbon was thus allowed to remain in place for all measurements. Good agreement with the theoretical plane Poiseuille profile of the two-layered flow was obtained. Some typical mean flow profiles are shown in non-dimensional form in figure 2. It may be noted that the mean flow profile is quite sensitive to the ratio of depths of the two layers and the ratio of the viscosities of the two liquids. Measurements of the mean flow in the transition range exhibited the typical flattening of the profiles.

Experiments were first carried out without excitation for a range of R_w. The hot-film was located at $X = 3{\cdot}5$ in., $Y = 0{\cdot}05$ in., $Z = 0$. For $R_w = 2000$ the residual motion u' was less than 0·05 % of the maximum mean flow velocity U_c, and was much less at low Reynolds numbers. Thus the flow could be said to be fully laminar up to $R_w = 2000$. As R_w was increased turbulent bursts or eddies began to appear. Further increase in the Reynolds number caused an increase in the frequency of bursts. Typical hot-film outputs for various values of R_w are shown in figure 3. Each interval of the time scale represents one second. Typical bursts appeared at $R_w = 2480$ and the frequency of bursts increased at $R_w = 2630$. Reynolds numbers for the oil (R_o) were less than 65 in all the experiments. Hot-film outputs for oil were not of much interest because of the low value of R_o.

We examined the nature and behaviour of sinusoidal disturbances introduced at different frequencies by means of the vibrating ribbon of the wave maker. The position of the ribbon was 0·05 in. from the bottom wall of the channel. It was found that a maximum displacement of amplitude of 0·0125 in. was satisfactory for the range of frequencies and Reynolds numbers explored.

The measurement of the amplitude of the damped disturbances excited by the vibrating ribbon was first carried out at low Reynolds numbers. The wave forms were quite pure and damped out quickly with distance downstream. The amplitude distributions of u'/U_c across the depth of the water phase for several distances downstream were measured and were symmetric with respect to the mid-depth of the water. The maximum peak remained essentially at a constant vertical location as the distance downstream varied. The damped modes in water

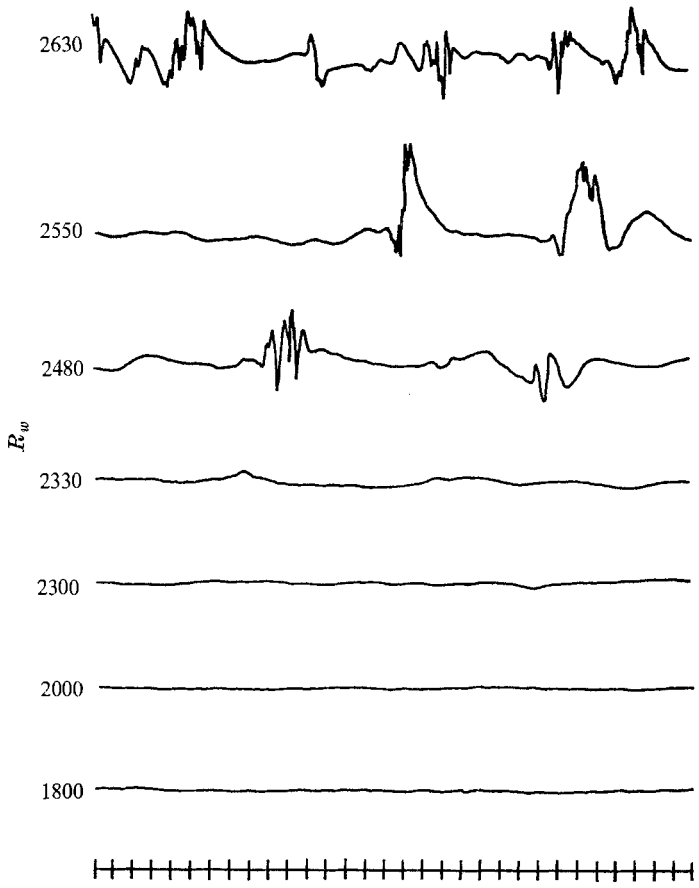

FIGURE 3. Natural disturbances at various Reynolds numbers of the water, R_w. Time between marks at bottom is 1 s. Time increases to the right.

behaved in much the same way as those found in Part 1. The interface was not disturbed at all, so that it behaved essentially like a rigid wall at these low Reynolds numbers. It should be emphasized, however, that at higher Reynolds numbers when the flow becomes unstable the interface participates in the instability and definitely does not behave like a rigid wall.

Figure 4 shows the amplitude distribution of u'/U_c for a typical damped disturbance at low Reynolds number ($R_w = 2120, R_o = 45, f = 1{\cdot}78$ Hz, $U_c = 5{\cdot}5$ in./s). The maximum value of u'/U_c was about $1{\cdot}0\,\%$. No secondary peaks are revealed in this case by taking depthwise data at points $0{\cdot}05\,Y/H$ apart.

An examination of phase changes with depth for damped modes was also undertaken. Phase shifts always occurred across the depth although the amplitude distributions were symmetric. Phase shifts of a disturbance along the vertical direction for a typical case are shown in figure 5 on a polar plot with phase uncertainties also indicated, following Hussain & Reynolds (1970). Note that the centre of the circle represents the bottom wall of the channel. The uncertainties

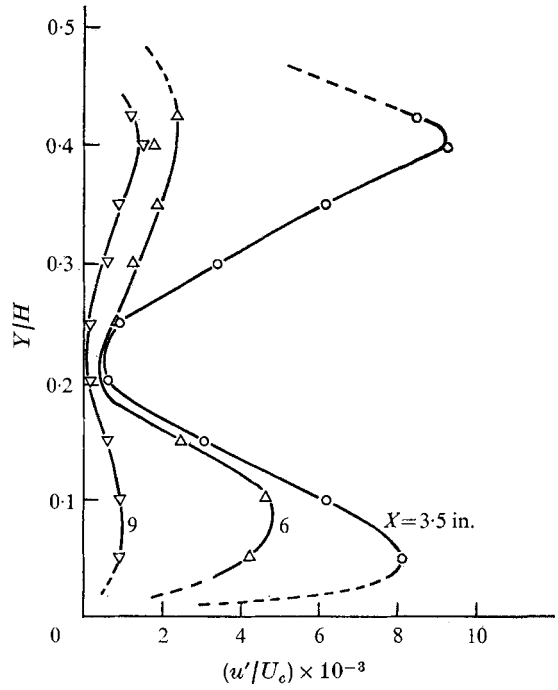

FIGURE 4. Vertical distribution of amplitude of disturbance with distance downstream for $R_w = 2120$, $R_o = 45$ and $f = 1{\cdot}78$Hz. ○, $X = 3{\cdot}5$ in.; △, $X = 6$ in.; ▽, $X = 9$ in.

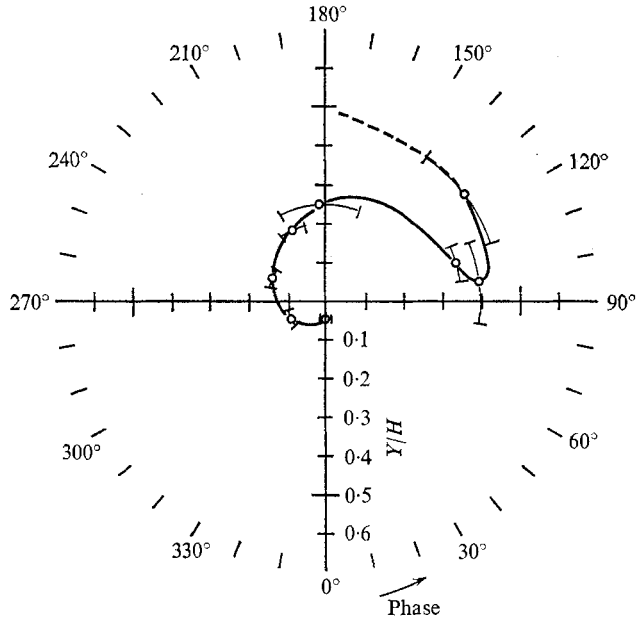

FIGURE 5. Vertical distribution of phase angle changes for $R_w = 2225$, $R_o = 44$, $X = 4{\cdot}5$ in., $f = 2{\cdot}83$ Hz. Bars denote phase uncertainties. Centre of circle represents the bottom wall of the channel.

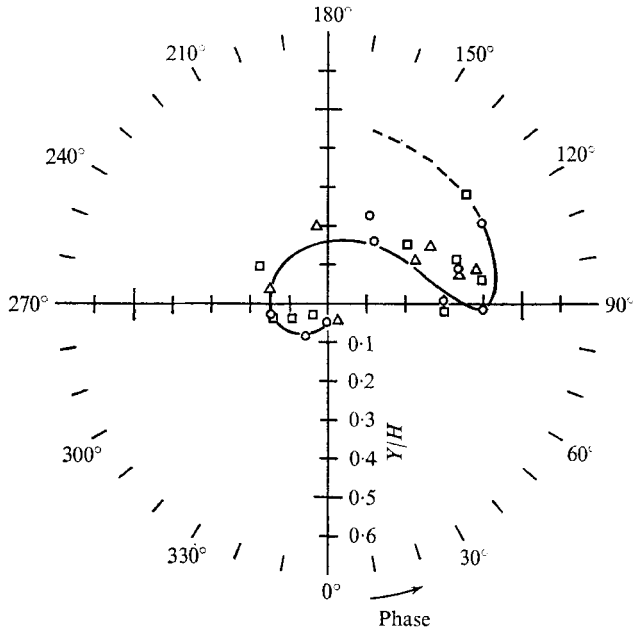

FIGURE 6. Phase angle changes downstream for $R_w = 2240$, $R_\theta = 46{\cdot}5$; ○, $X = 4{\cdot}25$ in.; △, $X = 6{\cdot}0$ in.; □, $X = 8{\cdot}0$ in., $f = 1{\cdot}78$ Hz.

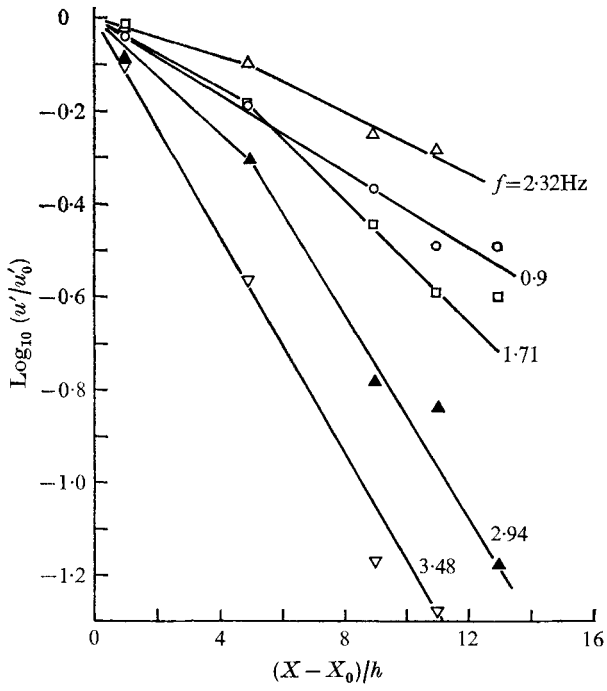

FIGURE 7. Decay of u' component of disturbances at $R_w = 2000$, $R_\theta = 39$; $X_0 = 3{\cdot}5$ in. ○, $f = 0{\cdot}9$ Hz; □, $f = 1{\cdot}71$ Hz; △, $f = 2{\cdot}32$ Hz; ▲, $f = 2{\cdot}94$ Hz; ▽, $f = 3{\cdot}48$ Hz.

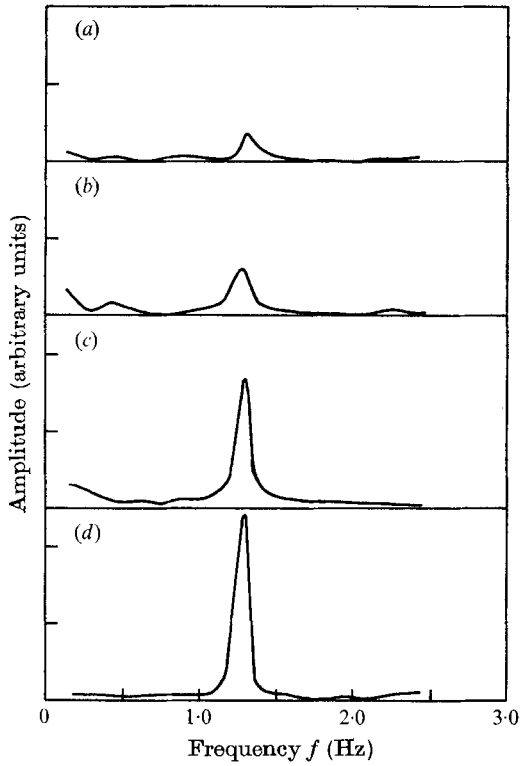

FIGURE 8. Spectra for a damped disturbance at $Y = 0{\cdot}05$ in., $R_w = 2000$, $R_o = 39$, $f = 1{\cdot}27$ Hz. (*a*) $X = 10$ in., (*b*) $X = 8$ in., (*c*) $X = 6$ in., (*d*) $X = 4$ in.

are seen to be substantial. It is noted that the disturbance in this figure is anti-symmetric in phase about the mid-depth of water. Figure 6 shows the phase distributions at different downstream stations. These are similar and they indeed fall around a single curve, indicating that there is no substantial phase velocity variation with depth and streamwise distances, so that at these distances away from the wave generator the mode corresponding to $\alpha = 1{\cdot}64 - 0{\cdot}07i$, $f = 1{\cdot}78$ Hz, $R_w = 2240$ appears to be predominant.

Typical decay behaviour at a fixed value of R_w for various frequencies, measured at $Y = 0{\cdot}05$ in. and various X with $X_0 = 3{\cdot}5$ in., is shown in figure 7 by plotting $\log_{10}(u'/u'_0)$ against $(X - X_0)/h$, where u'_0 is u' at $X = X_0$. The spectra of damped disturbances are similar to those obtained in Part 1 and are illustrated in figure 8, which shows a single dominant frequency. This fact and the exponential nature of the decay confirm the linearity of the disturbances. A large number of experiments were done in the damped region with similar results.

Further increase in Reynolds number into the range of transition of laminar flow to turbulent flow in water changed the shape of the amplitude distributions of u'/U_c markedly, as shown in figure 9. The interface was also noticeably wavy ($R_w = 2300$, $R_o = 48$, $f = 1{\cdot}74$ Hz, $U_m = 4{\cdot}33$ in./s). At a fixed frequency, slightly damped modes and a growing one were then excited. In contrast to the amplitude distributions of u'/U_c in the damped region, the shape here suggests the presence

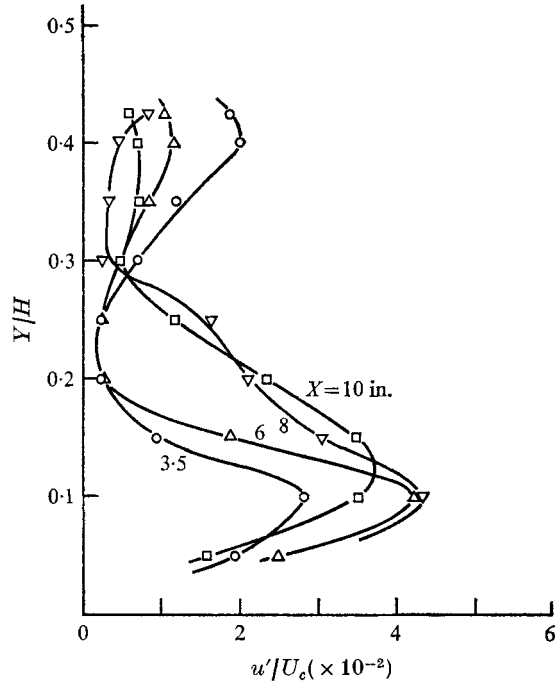

FIGURE 9. Vertical distribution of amplitude of disturbance with distance downstream for $R_w = 2300$, $R_o = 48$ and $f = 1{\cdot}74$ Hz. ○, $X = 3{\cdot}5$ in.; △, $X = 6$ in.; ▽, $X = 8$ in.; □, $X = 10$ in.

of several modes; this is typical of behaviour at the critical Reynolds number. It also appears that the viscosity of oil and the surface tension of the interface exert some stabilizing effect in addition to the smaller shear gradient of the mean flow near the interface, so that the amplitude distribution is very much skewed, with the maximum near the bottom wall. The lack of symmetry with respect to the mid-depth of water is also markedly different from the growing disturbances in the single fluid case of Part 1.

At values of R_w higher than 2300 both damped and growing disturbances were found. The growing disturbances increased in amplitude exponentially until breakdown occurred. The positions where linearity is preserved are dependent upon the frequencies excited by the artificial exciter. It appears that the location for initial breakdown X_b, when non-dimensionalized by the wavelength, is roughly proportional to the frequency, as shown in figure 10. From table 1 it is seen that the wavelength decreases with increase in frequency. Thus the growing long waves appear to have a higher tendency to break than short waves.

The presence of higher frequency components in the spectra of the disturbances indicates that breaking has occurred. The initial process of breakdown could be explained by following Benney & Lin (1960). The presence of the interface introduces another degree of freedom to random irregularity affecting the mean flow. This irregularity has a spanwise component which can give rise to the increased amplification rate of growing disturbances as suggested by Klebanoff & Tidstrom

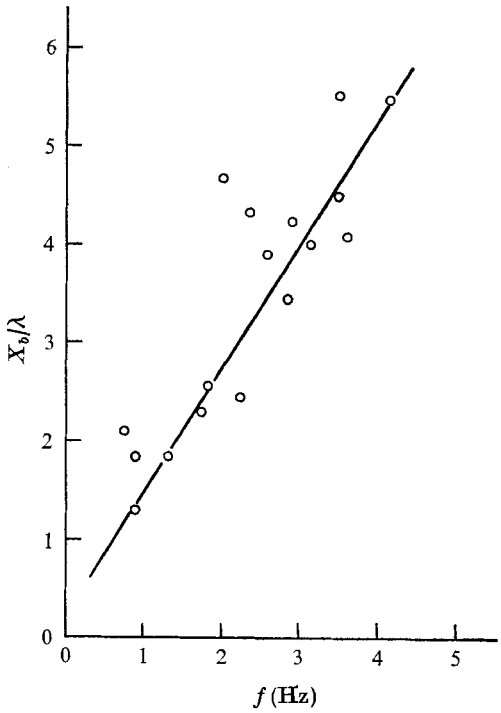

FIGURE 10. Breaking positions for growing disturbances with respect to excited frequencies.

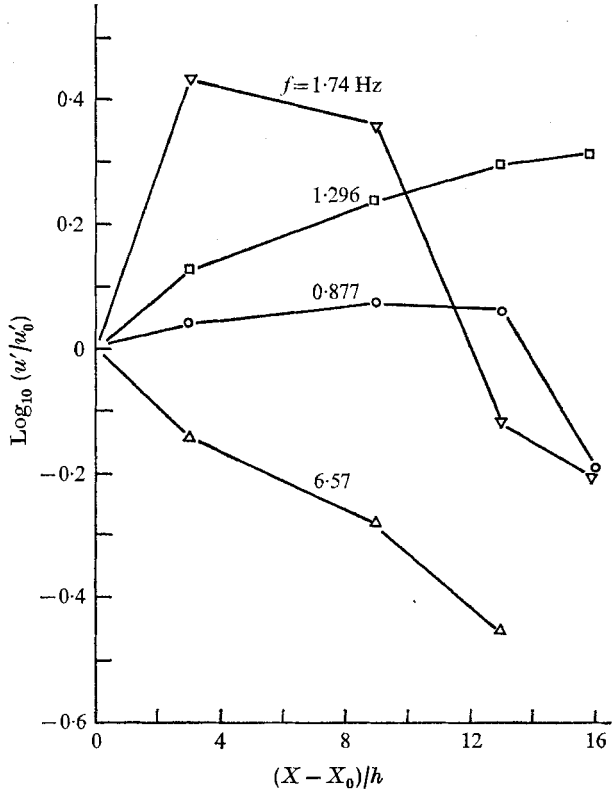

FIGURE 11. Decay and growth of u' component of disturbances at $R_w = 2330$, $R_o = 49$, $X_0 = 3{\cdot}5$ in. ○, $f = 0{\cdot}877$ Hz; □, $f = 1{\cdot}296$ Hz; ▽, $f = 1{\cdot}74$ Hz; △, $f = 6{\cdot}57$ Hz.

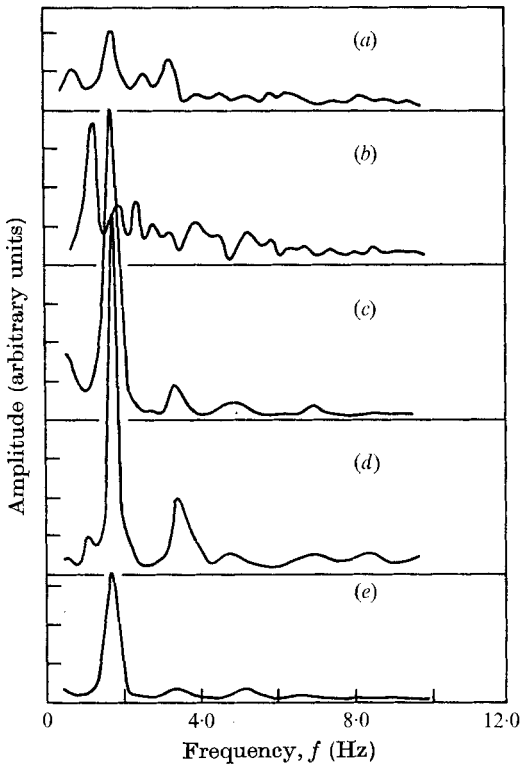

FIGURE 12. Spectra for a growing disturbance at $Y = 0{\cdot}05$ in., $R_w = 2330$, $R_a = 49$, $f = 1{\cdot}74$ Hz. (*a*) $X = 11{\cdot}5$ in., (*b*) $X = 10$ in., (*c*) $X = 8$ in., (*d*) $X = 5$ in., (*e*) $X = 3.5$ in.

(1959) for boundary-layer transition. The interaction of the originally two-dimensional waves with the three-dimensional disturbances develops the non-linear features. Thus higher frequency components than the basic one appear.

Figure 11 shows the typical decay and growth behaviours at a fixed Reynolds number for various frequencies, measured at $Y = 0{\cdot}05$ in. by plotting $\log_{10}(u'/u'_0)$ against $(X - X_0)/h$ with $X_0 = 3{\cdot}5$ in. The results show that, while most damped disturbances decay exponentially, the growing ones are somewhat less well behaved. For growing disturbances, linearity was preserved over a few wavelengths. As the Reynolds number was increased, outputs from the hot film were no longer pure. This is to be expected since the mean flow has natural disturbances other than those of the exciting frequency. The spectra of a growing and breaking disturbance at various positions downstream from the exciter are shown in figure 12.

A large number of experiments were carried out over a range of frequencies and Reynolds numbers, and the growth or decay and the wave speed were determined for each case. These are summarized on the $\beta/2\pi$ *vs.* R_w plot shown in figure 13. The plot exhibits a growing and a damped region which can be separated by a neutral stability boundary. The critical Reynolds number for water is 2300 and is in good agreement with the result of natural instability without artificial

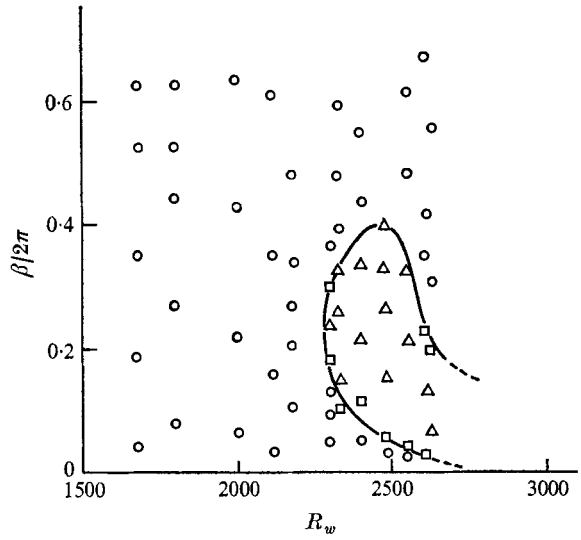

FIGURE 13. β, R_w plane showing regions of damping and growth, and the neutral stability boundary. ○, damped; △, growing; □, neutral.

excitations. With the wave speed known, the α_r, R_w plot was obtained as shown in figure 14. The least stable mode is at $\alpha_r = 1{\cdot}8$ and $R_w = 2280$. The results discussed in this paper were presented in a form that is directly comparable with the experiments of Charles & Lilleleht (1965). A further comparison with the results in Part 1 for a single fluid is also of interest and will now be made. For this purpose it is necessary to redefine a few of the non-dimensional numbers. First of all, the water Reynolds number is now defined as $R'_w = U_m d'/\nu_w$, where d' = wetted hydraulic diameter, so that $d = \frac{9}{17}d$ and $R'_w = \frac{18}{17}R_w$. The wavenumber is now defined as $\alpha'_r = (2\pi/\lambda)\,h'$, where h' is the half-depth of the water phase, i.e. $h' = \frac{1}{2}h$. It is then seen that the critical Reynolds number is $R'_{w,\,\mathrm{crit}} = 2430$, which is almost identical to that found for the one-layered case in Part 1. Also, since $\alpha'_r = \frac{1}{2}\alpha_r$, the region of instability in the wavenumber *vs.* Reynolds number plane is actually smaller than that in Part 1. The most unstable wavenumber is smaller, implying a longer wavelength than that for the most unstable wave in Part 1. The linearity of the amplified mode in this experiment was preserved for a shorter non-dimensional distance downstream than in the case of the single-fluid (water) experiment reported in Part 1. It should be noted that for this comparison the proper non-dimensional distance is obtained by normalizing the distance with the wavelength. Thus, for example, in Part 1, at $R = 2720$ and $f = 0{\cdot}87$Hz we have $X_b/\lambda = 5{\cdot}83$ whereas in the present case at $R'_w = 2470$ and $f = 0{\cdot}87$ Hz, $X_b/\lambda = 2{\cdot}16$, which is substantially smaller. Again in Part 1, at $R = 2720$ and $f = 1{\cdot}26$ Hz, $X_b/\lambda = 9{\cdot}58$ whereas here, at $R'_w = 2720$ and $f = 1{\cdot}28$ Hz, $X_b/\lambda = 1{\cdot}85$. It is obvious that the presence of the interface hastens the breakdown of the highly amplified disturbances. It may be pointed out again that since the interface participates in enhancing the instability the problem here, in the critical and unstable regimes, is not comparable to a Poiseuille–Couette flow.

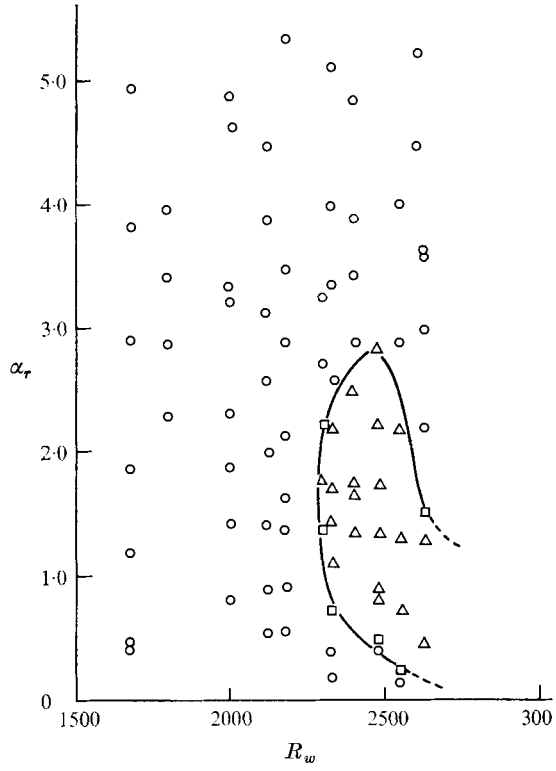

FIGURE 14. α_r, R_w plane showing regions of damping and growth, and the neutral stability boundary. ○, damped; △, growing; □, neutral.

Furthermore, the critical Reynolds number found here for the water phase is comparable to the single fluid case in Part 1 only in so far as it brings out the nature of the role of the interface.

Table 1 lists the values of frequency f, frequency parameter β, non-dimensional wave speed c/U_m (where c is the wave speed given by the formula $c = \lambda f$), non-dimensional wavenumber α_r and the amplification rate $-\alpha_i$, for various Reynolds numbers and values of U_m. It should be noted that the damping rate was calculated from the average of the damping rates at different X positions if these do not have the same value. The amplification rate was calculated similarly, but only up to the point of breakdown.

To excite the interfacial disturbances the position of the vibrating ribbon was changed to 0·4 in. from the bottom wall of the channel. The amplitude of the ribbon remained at 0·0125 in. as before. The amplitude distribution of disturbances was not symmetric. As the Reynolds number was increased, the unsymmetric character of the amplitude distributions became more noticeable and a truly interfacial mode was excited. As the Reynolds number was increased further, but before it reached its critical value, the disturbances near the interface could grow locally. However, such growth was preserved only for a very short distance and the wave was then damped out.

Figure 15 shows the amplitude distribution in water depthwise for several

R_w	R_o	U_m(in./s)	$f(Hz)$	β	c/U_m	α_r	$-\alpha_i$
1350	34	2·405	0·276	0·3606	0·767	0·47	−0·0308
			0·498	0·6503	0·811	0·805	−0·0456
			0·899	1·1718	0·956	1·125	−0·0880
			1·322	1·7278	0·968	1·78	−0·0497
			1·780	2·3185	0·974	2·39	−0·0653
			2·312	3·0222	0·943	3·21	−0·1407
			2·940	3·8390	0·957	4·01	−0·2564
			3·480	4·5364	0·962	4·37	−0·6107
2000	39	4·060	0·90	0·697	0·869	0·802	−0·0954
			1·27	1·021	0·722	1·415	−0·0476
			1·71	1·375	0·739	1·865	−0·0472
			2·32	1·785	0·788	2·31	−0·0405
			2·94	2·270	0·739	3·21	−0·1430
			3·48	2·689	0·805	3·34	−0·2678
			4·15	3·210	0·695	4·62	−0·3232
2330	50	4·33	0·458	0·3324	0·8395	0·396	−0·0059
			0·877	0·6365	0·8891	0·716	0·0059
			1·296	0·9406	0·8591	1·095	0·0500
			1·740	1·2622	0·8792	1·436	0·1989
			2·244	1·6279	0·9503	1·714	0·0892
			2·830	2·0533	0·9430	2·177	0·0428
			3·450	2·5032	0·9711	2·577	−0·0829
			4·130	2·9964	0·8949	3·349	−0·0548
			5·120	3·7146	0·9326	3·986	−0·0978
			6·570	4·7670	0·9296	5·125	−0·0852
2400	55	4·695	1·533	1·0260	0·7646	1·341	0·0369
			2·019	1·3508	0·8264	1·635	0·2565
			2·559	1·7121	0·9755	1·755	0·0497
			3·150	2·1080	0·8413	2·505	0·0801
			3·810	2·1281	0·8839	2·855	−0·1206
			4·130	2·7633	0·8051	3·433	−0·2618
			5·170	3·455	0·8860	3·907	−0·1844
			6·560	4·3894	0·9031	4·863	−0·2060
2480	57	4·33	0·284	0·2054	0·515	0·3995	—
			0·503	0·3644	0·755	0·4832	−0·0072
			0·898	0·6516	0·807	0·8076	0·0910
			1·322	0·9594	1·072	0·8976	0·0259
			1·775	1·2874	0·958	1·345	0·0471
			2·300	1·6688	0·9683	1·723	0·0272
			2·860	2·0753	0·9277	2·236	0·0513
			4·150	3·0109	0·8764	3·437	0·0414
2550	55	5·32	0·25	0·1476	1·0075	0·1465	−0·0264
			0·45	0·2657	1·066	0·2495	0·0019
			1·28	0·7558	1·043	0·7245	0·0119
			2·25	1·3288	1·034	1·285	0·3388
			3·48	2·0552	0·9398	2·186	0·0282
			5·12	3·0234	1·041	2·904	−0·0966
			6·55	3·8679	0·9624	4·017	−0·0704

TABLE 1. List of values of water Reynolds number, oil Reynolds number, average velocity of mean flow of water, frequency, frequency parameter, non-dimensional wave speed, non-dimensional wavenumber and amplification rate for small amplitude shear waves in water phase

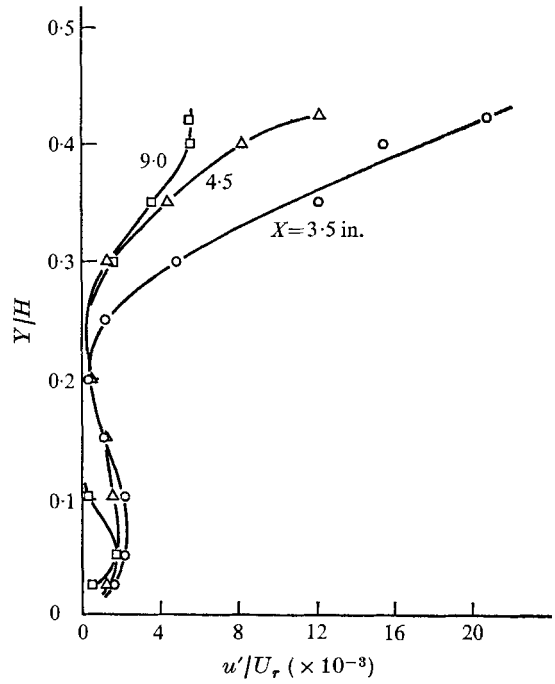

FIGURE 15. Vertical distribution of amplitude of disturbance with distance downstream for $R_w = 1760$, $R_o = 26$, $f = 2{\cdot}86$ Hz, when the ribbon was at $Y = 0{\cdot}4$ in. ○, $X = 3{\cdot}5$ in.; △, $X = 4{\cdot}5$ in.; □, $X = 9{\cdot}0$ in.

longitudinal distances downstream from the ribbon when the ribbon of the exciter was placed at $Y = 0{\cdot}4$ in. ($R_w = 1760$, $R_o = 26$, $f = 2{\cdot}86$ Hz). The amplitude is largest at the interface and decays rapidly away from it. This is significantly different from the shear modes in water in the damped region. The interface, of course, is now observably wavy. As seen in the figure, this mode is also damped even though it was artificially excited by the wave maker. The result shows that a truly interfacial mode could be excited by artificial means but is generally absent in natural transition, since no noticeable maximum in the amplitude distribution of the disturbance was observed at the interface in the transition range.

Disturbances at the interface of water and oil were studied by means of a wave gauge which was located downstream from the ribbon. Disturbances at the interface could also be observed visually. As the Reynolds number was increased to 2300 the outputs from the wave gauge began to show a little disturbance without artificial excitation. Charles & Lilleleht (1965) also observed interfacial disturbances around this Reynolds number. At higher Reynolds number the outputs of the wave gauge contained higher frequency disturbances.

With artificial excitation, there were two possibilities depending on whether the exciter was at $Y = 0{\cdot}05$ in. or $Y = 0{\cdot}40$ in. In the former case shear waves were excited in the water phase, and the waves at the interface, when they occurred in the transition range, were simply manifestations of these shear waves. In the latter case a truly interfacial mode was excited together with some vestiges

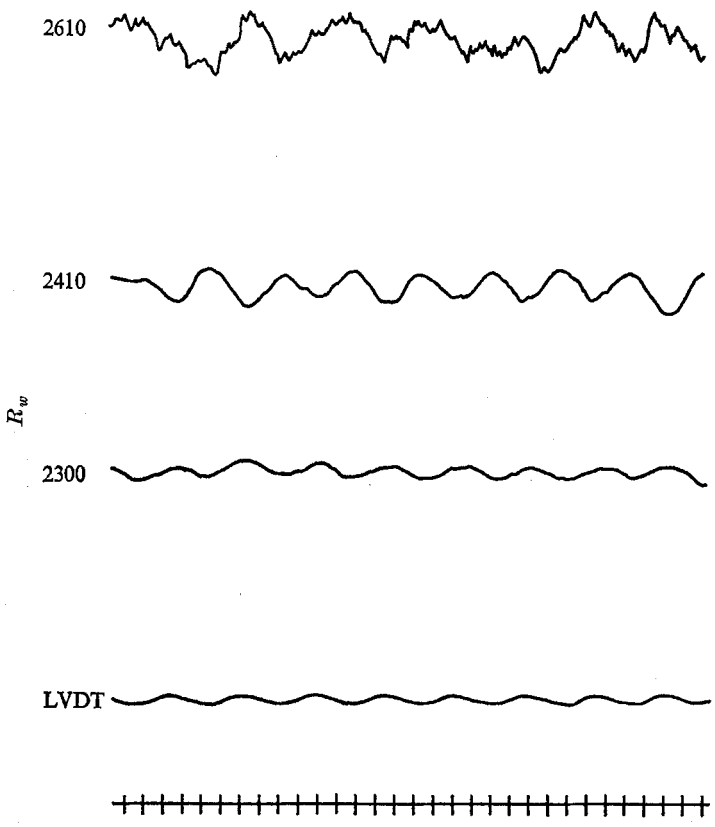

FIGURE 16. Voltage outputs from the wave gauge with $f = 0{\cdot}2374$ Hz for $R_w = 2300$, 2410 and 2610 at $X = 2{\cdot}75$ in. Lowest trace is signal from LVDT. Time between marks at bottom is 1 s. The ribbon of the wave maker was at $T = 0{\cdot}05$ in.

of shear waves. In figure 15 the shear modes can still be seen when the predominant interfacial mode is damped. In either case pure sinusoidal disturbances were obtained at low Reynolds numbers.

Figure 16 shows the outputs from the wave gauge when the flow was excited by the wave maker at a fixed frequency of 0·2374 Hz at different Reynolds numbers. The position of the ribbon was at $Y = 0{\cdot}05$ in. The lowest trace is for output from the LVDT as reference. Good sinusoidal disturbances were obtained at $R_w = 2300$ and $R_w = 2410$. The output at $R_w = 2610$ was almost the same as the output without excitation. The wave speed at the interface (c_f) with the ribbon at $Y = 0{\cdot}05$ in. was measured. This speed is in general greater than the interfacial mean velocity U_f and is almost the same as the speed of shear waves in the water phase. The agreement with the wave speed of the shear waves is on the average within about 15 %, which is about the order of errors in wave speed measurements.

Table 2 lists values of the non-dimensional wavenumber α_r, dimensionless interfacial wave speeds c_f/U_f and c_f/U_m, amplification rate $-\alpha_i$, exciting frequency f, average velocity of the mean flow of water U_m and the interfacial velocity U_f, for several Reynolds numbers.

R_w	R_o	U_f (in./s)	U_m (in./s)	f(Hz)	c_f/U_f	c_f/U_m	α_r	$-\alpha_i$
2310	48	2·7	4·348	0·458	1·020	0·635	0·532	−0·0810
				0·877	1·695	1·058	0·6016	−0·0446
				1·296	1·272	0·793	1·184	−0·0446
				1·740	1·695	1·058	1·1935	−0·1362
				2·244	1·695	1·058	1·5392	—
				2·83	1·020	0·635	3·233	−0·1362
				3·45	1·695	1·058	2·3665	−0·1258
				4·13	1·455	0·906	3·3014	−0·0446
2410	54	3·3	4·714	0·258	0·924	0·646	0·2658	−0·077
				0·476	1·250	0·875	0·3621	−0·0995
				1·089	1·111	0·777	0·9322	−0·118
				1·533	0·894	0·625	1·633	−0·218
				2·019	0·833	0·582	2·306	−0·281
				2·559	1·041	0·728	2·337	−0·770
				3·15	0·833	0·582	2·599	−0·026
				3·81	1·041	0·728	3·479	−0·026
				4·13	1·041	0·728	3·7717	−0·063
2480	57	2·94	4·329	0·2836	0·625	0·425	0·4842	−0·0745
				0·503	1·445	0·983	0·3718	0·318
				0·898	1·445	0·983	0·6637	0·0744
				1·322	1·445	0·983	0·9772	−0·1095
				1·775	1·030	0·699	1·840	−0·2310
				2·30	1·202	0·817	2·041	−0·1355
				2·86	1·445	0·983	2·114	−0·210
				3·50	1·445	0·983	2·587	−0·0744
				4·15	1·445	0·983	3·068	—

TABLE 2. List of values of water Reynolds number, oil Reynolds number, interfacial mean velocity, average velocity of mean flow of water, frequency, non-dimensional wave speed, non-dimensional wavenumber and amplification rate for small amplitude interfacial waves at interface of two fluids

These waves were, then, merely manifestations of the shear waves. Thus for natural transition truly interfacial waves were not excited. This is distinctly different from the case of the wind generated wave where the surface wave is excited through the Reynolds stress energy-transfer mechanism proposed by Miles (1957).

Figure 17 shows the outputs from the wave gauge when the position of the exciter was changed to $Y = 0{\cdot}4$ in. The wave gauge was moved downstream to $X = 5$, 6·75, 8·75 and 12·5 in. for $R_w = 1600$, $R_o = 26$, $f = 2{\cdot}8$ Hz. (At this low Reynolds number the wave gauge recorded no output when the ribbon was placed at $Y = 0{\cdot}05$ in.) Very pure sinusoidal damped disturbances were obtained.

The three-dimensionality of the disturbances was explored briefly in the same manner as in Part 1 and was found to be similar to those reported there. Figure 18 illustrates the two-dimensionality of a disturbance at $R_w = 750$ at two wavelengths downstream from the exciter. The hot-film outputs are from two probes placed 1 in. apart in the spanwise direction. Details of these results as well as numerous hot-film output signals, spectra and other data can be found in Park & Kao (1970).

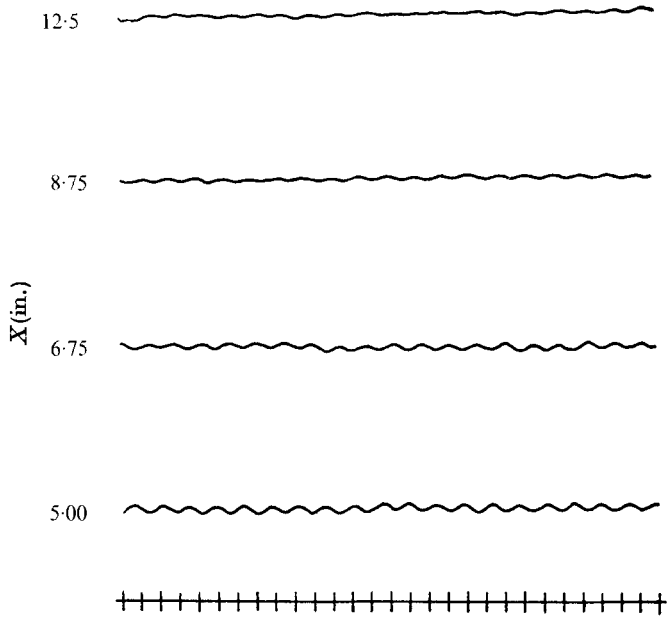

FIGURE 17. Wave gauge outputs for $f = 2{\cdot}80$ Hz, $R_w = 1600$, $R_o = 26$ at $X = 5{\cdot}0$, $6{\cdot}75$. $8{\cdot}75$, $12{\cdot}5$ in. when the ribbon was at $Y = 0{\cdot}4$ in. Time between marks at bottom is 1 s.

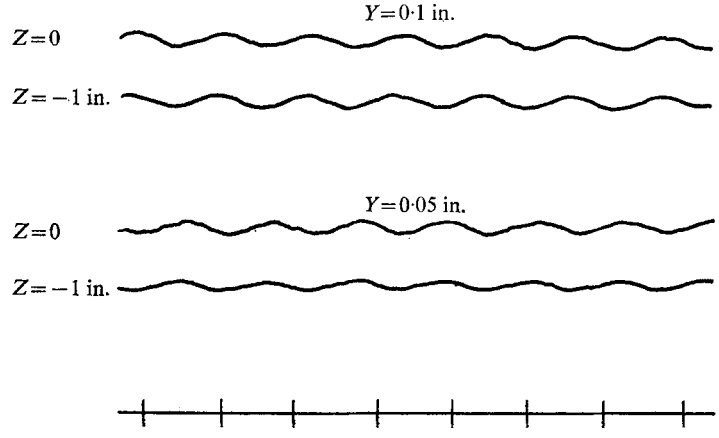

FIGURE 18. Hot-film outputs at $Z = 0$ and $Z = -1$ in. for $Y = 0{\cdot}1$ in. and $Y = 0{\cdot}05$ in. ($R_w = 750$, $R_o = 16$, $f = 0{\cdot}9$ Hz, $\lambda = 1{\cdot}71$ in.) Time between marks at bottom is 1 s.

4. Conclusions

(i) A critical water Reynolds number $R_w = 2300$ below which all small disturbances were damped and above which there were growing modes in water was found. From the controlled experiments, it was possible to obtain a well-defined neutral stability boundary in the β, R_w and α_r, R_w planes, separating regions of growth and decay. For $R_w > 2300$ the interface of the water and oil began to be disturbed. The value of the critical Reynolds number using artificial

excitation was in good agreement with the naturally occurring one. Oil Reynolds numbers were very low compared with water Reynolds numbers. The effect of the oil Reynolds number on the stability boundary is negligible.

(ii) It was found that the interface was undisturbed below the critical water Reynolds number. Furthermore, the effect of the interface on the characteristics of the disturbances in the water phase was negligible at low Reynolds number. In the fully damped region the disturbances in the water phase behaved very much like those in a rectangular channel with water alone, which in turn behaved very much like damped disturbances for plane Poiseuille flow. When the critical Reynolds number was reached the first manifestation of interfacial waves was also observed. For Reynolds numbers above the critical value, interfacial waves could be observed clearly without artificial excitation. It was shown by detailed measurements of the amplitude of the disturbances that the first appearance of interfacial waves was merely a manifestation of the shear waves. The truly interfacial mode was not excited. The waves therefore have the same three-dimensional nature as the shear waves in the water phase. These disturbances of the interface travel at the same speed as the shear waves. It was also found that this speed was faster than the interfacial mean velocity.

(iii) For fixed Reynolds numbers of the water above the critical value, the growth rate of disturbances was found to vary with frequency. Such disturbances occurred in the water phase only. Breakdown of a growing wave was found to occur in the form of a rapid simultaneous increase of various frequencies with a decrease in the amplitude of the dominant one. The water phase was thus in the transition range from laminar to turbulent flow while the oil phase remained laminar. The role of the interface at this stage was to introduce and enhance spanwise oscillations on the water phase and thus to hasten the process of breakdown for growing disturbances in the water phase.

(iv) When the ribbon was placed near the interface, the shear modes were not strongly excited and forced excitation of a truly interfacial mode was obtained. Shear waves were excited when the ribbon was placed near the bottom wall. In natural transition the interfacial mode was not excited.

(v) Most of the excited disturbances quickly achieved three-dimensionality except at very low Reynolds numbers, where two-dimensionality was preserved for several wavelengths. This three-dimensionality was enhanced by the extra degree of freedom of the interface.

The authors are indebted to the National Science Foundation for their support under grant GK-2639.

REFERENCES

ANDREAS, J. M., HAUSER, E. A. & TUCKER, W. B. 1938 *J. Phys. Chem.* **42**, 1001.

BENNEY, D. J. & LIN, C. C. 1960 *Phys. Fluids*, **3**, 656.

CHARLES, M. E. & LILLELEHT, L. U. 1965 *J. Fluid Mech.* **22**, 217.

FORDHAM, S. 1948 *Proc. Roy. Soc.* A **194**, 1.

HUSSAIN, A. K. M. F. & REYNOLDS, W. C. 1970 *J. Fluid Mech.* **41**, 241.

KAO, T. W. & PARK, C. 1970 *J. Fluid Mech.* **43**, 145–164.

KING, H. W. 1954 *Handbook of Hydraulics*, 4th edn. McGraw-Hill.

KLEBANOFF, P. S. & TIDSTROM, K. D. 1959 *N.A.S.A. Tech. Note*, no. D-195.

LOCK, R. C. 1954 *Proc. Camb. Phil. Soc.* **50**, 105.

MILES, J. W. 1957 *J. Fluid Mech.* **3**, 185.

PARK, C. & KAO, T. W. 1970 *Dept. of Space Science and Applied Physics, The Catholic University of America Tech. Rep.* no. 70-006.

TANG, Y. P. & HIMMELBLAU, D. M. 1963 *Chem. Eng. Sci.* **18**, 143.

YIH, C.-S. 1967 *J. Fluid Mech.* **27**, 337.